Journal of Sound and Vibration (1998) **212**(1), 23–36

MACH NUMBER DEPENDENCE OF THE COMPRESSION WAVE GENERATED BY A HIGH-SPEED TRAIN ENTERING A TUNNEL

M. S. Howe

Boston University, *College of Engineering*, 110 *Cummington Street*, *Boston*, *MA* 02215, *U.S.A.*

(*Received* 11 *June* 1997, *and in final form* 3 *October* 1997)

An analysis is made of the compression wave generated when a high speed train enters a tunnel. Operations in the near future are expected to be at Mach numbers M ranging in value up to 0·4. Non-linear steepening of the wave in a very long tunnel exacerbates the environmental damage caused by the subsequent radiation of an inpulsive *micro-pressure wave* from the far end of the tunnel. The compression wave profile depends on train speed and the area ratio of the train and tunnel, and for $M < 0{\cdot}2$ can be estimated to a good approximation by regarding the local flow near the tunnel mouth during train entry as *incompressible*. The influence of higher train Mach numbers is investigated for the special case in which the tunnel is modelled by a thin-walled circular cylinder, of the type frequently used in model scale tests. This is done by representing the nose of the train by a distribution of monopole sources, and calculating their interaction with the mouth of the tunnel by using the exact acoustic Green's function for a semi-infinite, circular cylindrical tunnel. Empirical formulae valid up to $M = 0{\cdot}6$ are obtained for the compression wave amplitude and for the maximum *initial* pressure gradient (which determines the amplitude of the micro-pressure wave). Predictions of the theory are found to be within 5% of measurements made in recent experiments.

1. INTRODUCTION

The amplitude of the compression wave produced when a high speed train enters a tunnel depends principally on the speed U of the train at the tunnel entrance and on the ratio $\mathscr{A}_o/\mathscr{A}$ of the train cross-sectional area $\mathscr{A}_o$ to that of the tunnel $\mathscr{A}$ [1–10]. The wave propagates one-dimensionally ahead of the train at about the speed of sound c_o. When $\mathscr{A}_0/\mathscr{A} \ll 1$ and for train Mach numbers $M \equiv U/c_o < 0{\cdot}2$, the pressure rise across the wave is approximately equal to $\rho_o U^2 \mathscr{A}_o/\mathscr{A} \sim M^2(\mathscr{A}_o/\mathscr{A})p_o$, where ρ_o and p_o are, respectively, the mean air density and pressure, which typically is of the order of 1 % of atmospheric pressure. Part of the wave energy is radiated from the far end of the tunnel as a spherically spreading pulse, known as the *micro-pressure wave* [1, 2]. In a very long tunnel (3 km or more in length) with concrete slab track, non-linear steepening of the compression wave can result in micro-pressure wave amplitudes (proportional to the compression wave pressure gradient at the end of the tunnel) in excess of 1 lb/ft^2 near the tunnel exit, which is comparable to the disturbance produced by the sonic boom from a supersonic aircraft. The minimization of the environmental damage caused by micro-pressure waves (first recognized in Japan in 1975) requires, in the first instance, a proper understanding of the mechanism of compression wave generation [3, 11].

0022–460X/98/160023 + 14 $25.00/0/sv971348

The wave is generated by the interaction of the non-uniform pressure field of the train (which is *frozen* in a frame fixed with a uniformly translating train) with the tunnel entrance. At Mach numbers less than about 0·2, the compression wave thickness is very much larger than the tunnel entrance diameter, and the local motion in the neighborhood of the tunnel mouth during the interaction is effectively the same as if the fluid were incompressible. In this limit, it was shown in reference [10] that the wave generated by tunnel entrance "scattering" can be expressed in terms of a simple, general formula (in which the influence of tunnel inlet geometry is specified independently of the subsequent propagation of the wave within the tunnel) involving the convolution product of a *compact* Green's function with a distribution of sources representing the moving train. According to this approach, the influence of tunnel entrance geometry is completely defined by a velocity potential (solution of Laplace's equation) describing a hypothetical incompressible flow from the tunnel mouth.

Future high speed trains (including "MAGLEV" systems) are expected to operate at Mach numbers approaching 0·4 [12]. The influence of compressibility on train-mouth "scattering" will then be significant, and the simple theory of reference [10] will supply only a crude first approximation. In these circumstances, the theory of compression wave generation can be developed formally as in the low Mach number limit, but the tunnel mouth velocity potential must now be determined from the solution of the acoustic wave equation rather than Laplace's equation. This potential can be obtained for any particular tunnel entrance geometry by numerical integration, and can incorporate such effects as, for example, the presence of steep-sided cuttings extending outward from the tunnel portal. However, it is often desirable to have predictions in analytical form for specific tunnel geometries. These can be used to benchmark numerical solutions, and to make preliminary estimates at high Mach numbers. Recent numerical and experimental studies have involved axisymmetric scale model trains projected at high speed along the axis of symmetry of a tunnel consisting of a long cylinder of circular cross-section [4–8]. The exact acoustic Green's function is known for this geometry, and is applied in this paper to obtain an analytic representation of compression wave generation.

To do this, a circular symmetric "train" is represented by a continuous distribution of monopole sources along its axis of symmetry. For the slender nose profiles used in the experiments, which are characteristic of modern high speed locomotives, the source density is locally proportional to the rate of change of cross-sectional area of the train with distance from the nose. The adequacy of this approximation is confirmed by the results of full numerical simulations of the tunnel entry problem and by model tests when $\mathscr{A}_o/\mathscr{A} \leqslant 0{\cdot}2$ [4, 5]. The dependence of the compression wave on Mach number is then determined by making use of Green's function for a semi-infinite circular cylinder. Results are given for a train with a snub nose, which can be modelled by a translating point source, and these are used to determine the Mach number dependence of both the compression wave amplitude and the peak pressure gradient. Application is also made to axisymmetric model trains with conical, parabolic and elliptic nose profiles; absolute predictions of the compression wave gradient (that ultimately controls the magnitude of the micro-pressure wave) are within 5% of corresponding experimental data given in reference [4].

The analytical problem is formulated and solved in section 2 in terms of the Green's function for a semi-infinite rigid cylinder. The snub nosed train modelled by a point source is discussed in section 3, where simple empirical formulae are obtained for the Mach number dependence of the peak pressure and pressure gradient, and a comparison made with the zero Mach number theory of reference [10]. In section 4 application is made to model train nose profiles studied in reference [4], and a comparison made with that experiment.

2. THE CIRCULAR CYLINDRICAL TUNNEL

2.1. FORMULATION

The model experiments conducted by Maeda *et al*. [4] involve the projection of axisymmetric model "trains" along the axis of a tunnel formed by a long, thin-walled circular cylinder. The generation of the compression wave in this case will be investigated analytically by considering a semi-infinite, *unflanged* circular cylindrical tunnel of radius R ($\mathscr{A} = \pi R^2$), that extends along the negative x-axis of the rectangular system $\mathbf{x} = (x, y, z)$, with the co-ordinate origin O taken on the axis of symmetry in the plane of the tunnel mouth (see Figure 1). Let the train enter the tunnel at constant speed U. The train cross-section is taken to be constant and of area $\mathscr{A}_o \equiv \pi h^2$ at a distance L from the nose, where h is its maximum radius. In typical applications the ratio $\mathscr{A}_o/\mathscr{A}$ is small.

The nose profile is assumed to be streamlined and the aspect ratio h/L sufficiently small to ensure that flow separation does not occur. The displacement of air by the moving train may then be represented by a distribution of time-independent, monopole volume sources convecting in the negative x-direction at the speed U of the train. The source strength will be denoted by $q(x + Ut, y, z)$, where $q(\mathbf{x})$ is the source distribution at time $t = 0$, when the nose of the train will be supposed to enter the tunnel. The monopoles are non-zero only in the vicinities of the nose and tail of the train, where the cross-sectional area varies. When $\mathscr{A}_o/\mathscr{A}$ is small, it was shown in reference [10] that q can be approximated by a *line source* on the axis of symmetry of the train, namely

$$q(\mathbf{x}) = U\mathscr{A}_o Q(x)\delta(y - y_T)\delta(z), \qquad Q(x) = \frac{1}{\mathscr{A}_o}\frac{\partial \mathscr{A}_T}{\partial x}(x), \tag{1}$$

where $\mathscr{A}_T(x)$ is the train cross-section at distance x from the nose (so that $\mathscr{A}_T(L) \equiv \mathscr{A}_o$) and, for generality, the axis of the train is permitted to be offset a distance y_T from the tunnel axis.

The motion of the air produced by these sources is described by a velocity potential $\phi(\mathbf{x}, t)$, which satisfies the inhomogeneous acoustic equation

$$\left(\frac{1}{c_0^2}\frac{\partial^2}{\partial t^2} - \nabla^2\right)\phi = -q(x + Ut, y, z), \tag{2}$$

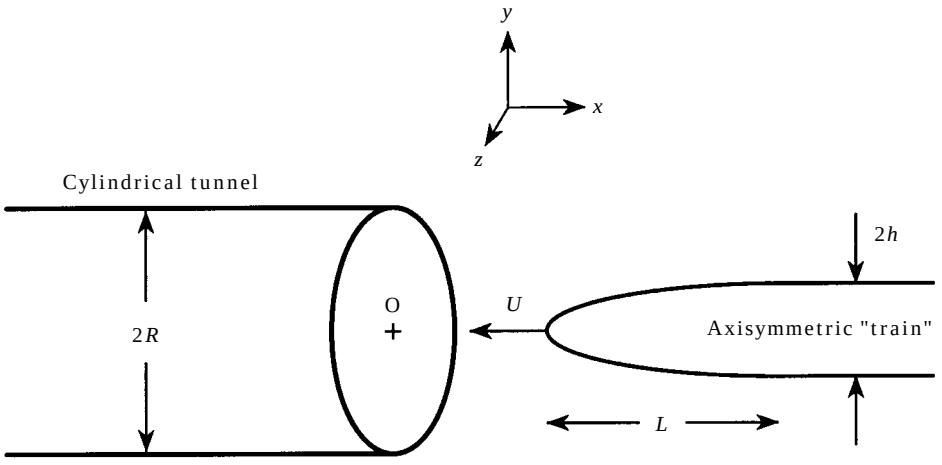

Figure 1. Axisymmetric model train projected along the axis of symmetry of a circular cylindrical tunnel.

where the normal derivative $\partial\phi/\partial x_n = 0$ on the interior and exterior circular cylindrical tunnel walls. The solution of this equation is written

$$\phi(\mathbf{x}, t) = -\int\int G(\mathbf{x}, \mathbf{x}'; t-\tau) q(\mathbf{x}', \tau)\, \mathrm{d}^3\mathbf{x}'\, \mathrm{d}\tau, \qquad \mathbf{x}' = (x', y', z'), \tag{3}$$

where $G(\mathbf{x}, \mathbf{x}'; t-\tau)$ is Green's function, which is the solution of equation (2) with outgoing wave behaviour when the right hand size is replaced by $\delta(\mathbf{x}-\mathbf{x}')\delta(t-\tau)$. G is required to satisfy $\partial G/\partial x_n = 0$ and $\partial G/\partial x_n' = 0$ when the field points $\mathbf{x}$, $\mathbf{x}'$ lie respectively on the tunnel walls, and the integrations in equation (3) are over the whole of the fluid and all times $\boldsymbol{\tau}$. It may be remarked that the formal representation (3) is also applicable for more complex interaction problems, for example, when two trains travelling in opposite directions pass in the neighborhood of the tunnel entrance (although this would require modification of boundary conditions).

Equation (2) is applicable within the tunnel only when the progressive, non-linear steepening of the compression wave front is ignored. Steepening is important in long tunnels, but only at large distances in front of the train. Within an extensive intermediate region, many tunnel diameters ahead of the train, the unsteady motion is one-dimensional and of small amplitude, and the perturbation pressure $p(x, t)$ is given to a good approximation by the linearized Bernoulli equation $p = -\rho_o\, \partial\phi/\partial t$.

The *micro-pressure wave* $p'(\mathbf{x}, t)$ radiated from the far end of the tunnel (at $x = x_E$, say) when the compression wave arrives, is given in a crude first approximation by [3, 13, 14]

$$p'(\mathbf{x}, t) \approx \frac{\mathscr{A}}{\Omega c_o \wp} \frac{\partial p}{\partial t}(x_E, t - \wp/c_o), \qquad \wp \gg R, \tag{4}$$

at distance $\wp$ from the tunnel exit, where Ω is the effective solid angle into which the wave radiates (which depends on local conditions, such as the presence of embankments, etc., near the exit). Because of non-linear steepening, the value of the derivative on the right-hand side cannot normally be evaluated from the linear theory pressure determined from equation (3). However, the solution (3) determines the initial waveform that defines initial conditions for a one-dimensional, non-linear model of propagation that can be used to determine the pressure at the far end of the tunnel, although this aspect of the problem is not discussed here.

2.2. GREEN'S FUNCTION

The calculation of Green's function is simplified by noting that, in practice, it is required to calculate the compression wave only at large distances from the tunnel mouth, where three-dimensional features of the solution (which decay exponentially fast with distance into the tunnel) are negligible. Thus it may be assumed that the field point $\mathbf{x}$ in equation (3) lies within the tunnel at $|x| \gg R$. The functional form of G may then be deduced from standard results given by Noble [15].

If we set

$$G(\mathbf{x}, \mathbf{x}'; t-\tau) = -\frac{1}{2\pi}\int_{-\infty}^{\infty} \bar{G}(\mathbf{x}, \mathbf{x}'; \omega) \mathrm{e}^{-i\omega(t-\tau)}\, \mathrm{d}\omega, \tag{5}$$

then $\bar{G}$ satisfies the inhomogeneous Helmholtz equation $(\nabla^2 + \kappa_0^2)\bar{G} = \delta(\mathbf{x}-\mathbf{x}')$, $\kappa_o = \omega/c_o$. The characteristic frequency of the compression wavefront prior to steepening $\sim U/2R$, so that for $M < 0{\cdot}6$, $\kappa_o R \leqslant 1{\cdot}89 < 3{\cdot}83$. This condition ensures that the acoustic motions

within the tunnel consist primarily of axially propagating plane waves [15]. In practice the principal compression wave frequency rarely exceeds about 20 Hz, and $\kappa_o R < 1{\cdot}7$.

To calculate the field $\bar{G}(\mathbf{x}, \mathbf{x}'; \omega)$ produced by the point source $\delta(\mathbf{x} - \mathbf{x}')$ at $\mathbf{x}'$ when the observation point $\mathbf{x}$ is within the tunnel, far from the mouth, we consider the *reciprocal* problem in which the source is regarded as placed at $\mathbf{x}$ and the solution $\bar{G}(\mathbf{x}', \mathbf{x}; \omega)$ is found as a function of $\mathbf{x}'$, where $\mathbf{x}'$ may be regarded as located in the vicinity of the tunnel mouth. According to the reciprocal theorem $\bar{G}(\mathbf{x}', \mathbf{x}; \omega) = \bar{G}(\mathbf{x}, \mathbf{x}'; \omega)$ [13].

Only plane waves can propagate when $\kappa_o R < 3{\cdot}8$, so that the reciprocal source at $\mathbf{x}$ generates the plane wave $e^{i\kappa_0(x' - x)}/2i\kappa_o \mathscr{A}$ which is incident on the tunnel mouth from $x' < 0$. We therefore write, near the tunnel entrance,

$$\bar{G}(\mathbf{x}', \mathbf{x}; \omega) = \frac{e^{-i\kappa_o x}}{2i\kappa_o \mathscr{A}} \{e^{i\kappa_o x'} + \Psi(\mathbf{x}'; \omega)\} \tag{6}$$

where the function $\Psi(\mathbf{x}'; \omega)$ represents the influence of the mouth, including radiation losses into free space. Noble (reference [15], section 3.4) shows that, for $r' \equiv \sqrt{(y'^2 + z'^2)} < R$,

$$\Psi(\mathbf{x}'; \omega) = \frac{i\kappa_o R \mathscr{K}_+(\kappa_o)}{2\pi} \int_{-\infty}^{\infty} \frac{I_0(\gamma r') \mathscr{K}_-(k)}{\gamma I_1(\gamma R)} e^{ikx'} \, dk, \tag{7}$$

where I_0, I_1 are modified Bessel functions (reference [16], section 9.6). The function $\gamma = \sqrt{(k^2 - \kappa_0^2)}$ has branch cuts extending from $k = \pm\kappa_o$ to $\pm i\infty$, respectively, in the upper and lower halves of the complex k-plane, such that on the real axis, γ is real and positive when $|k| > |\kappa_o|$, and $\gamma = -i\,\mathrm{sgn}\,(\kappa_o)\sqrt{(\kappa_0^2 - k^2)}$ for $|k| < |\kappa_o|$. The functions $\mathscr{K}_\pm(k)$ are respectively regular and non-zero in Im $k \gtrless 0$, and satisfy

$$\mathscr{K}_+(k)\mathscr{K}_-(k) = 2I_1(\gamma R)K_1(\gamma R), \qquad \text{for real } k,$$

where K_1 is a modified Bessel function. In all of these formulae, divergent integrals are avoided by assigning to ω a small positive imaginary part which is subsequently allowed to vanish. This ensures that $\Psi(\mathbf{x}'; \omega)$ satisfies the radiation condition.

The substitution of these expressions into the right-hand side of equation (5) supplies the Green's function in the form

$$G(\mathbf{x}, \mathbf{x}'; t - \tau) = G_o(x, x'; t - \tau) + G_s(\mathbf{x}, \mathbf{x}'; t - \tau), \tag{8}$$

such that, for $x < x'$ within the tunnel,

$$G_o(x, x'; t - \tau) = \frac{c_o}{2\mathscr{A}} H\left(t - \tau + \frac{x - x'}{c_o}\right),$$

$$G_s(\mathbf{x}, \mathbf{x}'; t - \tau) = \frac{-R}{8\pi^2 \mathscr{A}} \int\int_{-\infty}^{\infty} \frac{I_0(\gamma r') \mathscr{K}_+(\kappa_o) \mathscr{K}_-(k)}{\gamma I_1(\gamma R)} e^{-i\omega(t - \tau + x/c_o) + ikx'} \, dk \, d\omega, \tag{9}$$

where $H(x) = 0$, 1 accordingly as $x \lessgtr 0$ is the Heaviside step function.

2.3. THE COMPRESSION WAVE

The pressure wave $p(x, t)$ radiated ahead of the train as it enters the tunnel may now be calculated by use of equations (1), (3), (9) and the relation $p = -\rho_o \, \partial\phi/\partial t$. However, the integration with respect to k in the definition (9) of $G_s(\mathbf{x}, \mathbf{x}'; t - \tau)$ must be evaluated numerically, and the computations are simplified (because singularities on the real k-axis

as $\mathrm{Im}\,\omega \to +0$ are then absent) if we first calculate numerically the compression wave pressure *gradient* $\partial p(x, t)/\partial t$, and then use

$$p(x, t) = \int_{-\infty}^{t} \frac{\partial p}{\partial t'}(x, t')\,\mathrm{d}t'. \tag{10}$$

When the various integrations are cast in non-dimensional forms, we find

$$\left(\frac{R\mathscr{A}}{\rho_o U^3 \mathscr{A}_o}\right)\frac{\partial p}{\partial t}(x, t) = \frac{1}{2\pi\sqrt{(1-M^2)}}\int_0^\infty \frac{\lambda I_0((\lambda y_T/R)\sqrt{(1-M^2)})}{I_1(\lambda\sqrt{(1-M^2)})}$$

$$\times\ \mathrm{Re}\left\{\bar{Q}(\lambda)\mathscr{K}_+\left(\frac{\lambda M}{R}\right)\mathscr{K}_-\left(\frac{\lambda}{R}\right)\mathrm{e}^{-i\lambda U[t]/R}\right\}\mathrm{d}\lambda, \tag{11}$$

where $y_T < R$ is the offset between the axes of the train and tunnel, $[t] = t + x/c_o$ is the retarded time, and

$$\bar{Q}(\lambda) = \int_{-\infty}^{\infty} Q(x')\mathrm{e}^{i\lambda x'/R}\,\mathrm{d}x'. \tag{12}$$

The functions $\mathscr{K}_+(\lambda M/R)$ and $\mathscr{K}_-(\lambda/R)$ are evaluated by the Cauchy integral method described by Noble [15] from the formulae

$$\mathscr{K}_+(\lambda M/R) = \exp\left\{\frac{-i\lambda M}{\pi}\int_0^\infty \frac{\ln\left[2I_1(\sqrt{(\mu^2-\lambda^2M^2)})K_1(\sqrt{(\mu^2-\lambda^2M^2)})\right]}{\mu^2-\lambda^2M^2}\,\mathrm{d}\mu\right\},$$

$$\mathscr{K}_-(\lambda/R) = \sqrt{2I_1(\lambda\sqrt{(1-M^2)})K_1(\lambda\sqrt{(1-M^2)})}$$

$$\times\exp\left\{\frac{i\lambda}{\pi}\int_0^\infty \ln\left[\frac{I_1(\sqrt{(\mu^2-\lambda^2M^2)})K_1(\sqrt{(\mu^2-\lambda^2M^2)})}{I_1(\lambda\sqrt{(1-M^2)})K_1(\lambda\sqrt{(1-M^2)})}\right]\frac{\mathrm{d}\mu}{\mu^2-\lambda^2}\right\}, \tag{13}$$

where, in the interval $0 < \mu < M\lambda$,

$$I_1(\Gamma)K_1(\Gamma) = -\frac{\pi}{2}(J_1(|\Gamma|)Y_1(|\Gamma|) - iJ_1^2(|\Gamma|)), \qquad \Gamma = \sqrt{(\mu^2-\lambda^2M^2)},$$

J_1, Y_1 being ordinary Bessel functions [16].

3. SNUB NOSED TRAIN MODELLED BY A POINT SOURCE

3.1. MACH NUMBER DEPENDENCE

Consider a long, snub nosed train entering the tunnel, for which the aspect ratio h/L is very large. In the limit $L \to 0$, the source density $Q(x) \equiv (1/\mathscr{A}_o)\,\partial\mathscr{A}_T/\partial x \to \delta(x)$, and the nose of the train becomes equivalent to a single point source $q(\mathbf{x}) = \mathscr{A}_o U\delta(\mathbf{x})$ of strength $\mathscr{A}_o U$. When the train travels along the axis of symmetry of the tunnel, the compression wave pressure gradient $\partial p/\partial t$ is calculated from equation (11) by setting $y_T = 0$ and $\bar{Q}(\lambda) = 1$. The pressure gradient and the compression wave profile $p(x, t)$ (obtained from equation (10)) are plotted against $U[t]/R$ in Figure 2 for Mach numbers M between 0·1 and 0·4. These results confirm that the compression wave *rise time* is essentially independent of Mach number (i.e., of the compressibility of the motion in the

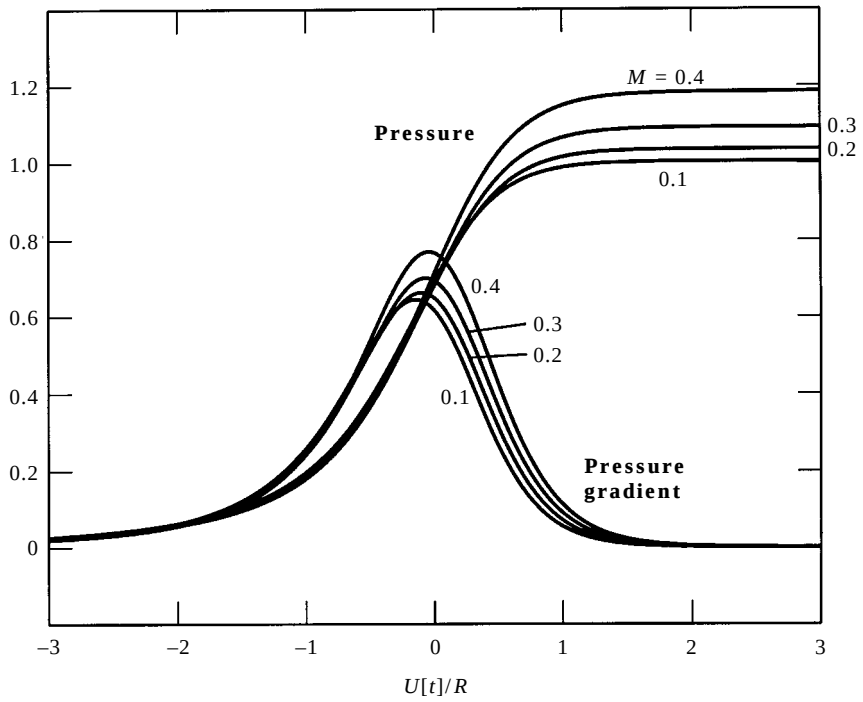

Figure 2. Pressure wave $p/(\rho_o U^2 \mathscr{A}_o/\mathscr{A})$ and pressure gradient $(\partial p/\partial t)/(\rho_o U^3 \mathscr{A}_o/R\mathscr{A})$ profiles generated by a snub nosed train approximated by a point source for different Mach numbers $M = U/c_o$.

neighbourhood of the tunnel mouth), being equal to the effective transit time $\sim 2R/U$ of the nose across the entrance plane of the tunnel.

The net pressure rise Δp, say, across the wave front is given by the limiting value of the integral in equation (10) as $t \to \infty$. This integral yields a δ-function $\delta(\lambda)$ when the representation (11) of $\partial p/\partial t'$ is used. Since $\mathscr{K}_{\pm}(k) \to 1$ as $k \to 0$ (reference [15], section 3.4), it then follows that

$$\Delta p = \frac{\rho_o U^2 \mathscr{A}_o/\mathscr{A}}{1 - M^2}. \tag{14}$$

This formula is actually valid for *any* train profile when the equivalent source distribution is approximated as in equation (1), because in all cases $\bar{Q}(\lambda) \to 1$ as $\lambda \to 0$. The dependence of Δp on M predicted by numerical evaluation of equations (10) and (11) is plotted as the solid curve in Figure 3 for comparison with equation (14) (shown dotted).

The rate of non-linear steepening of the compression wave in a long tunnel depends critically on the initial value of the maximum pressure gradient $(\partial p/\partial t)_{max}$. This is also plotted (for the point source/snub nose approximation) as a solid curve in Figure 3. It is well approximated by the empirical formula (dotted in the figure)

$$\left(\frac{\partial p}{\partial t}\right)_{max} = \left(\frac{\rho_o U^3 \mathscr{A}_o}{R\mathscr{A}}\right) \frac{0{\cdot}64 + 1{\cdot}3M^6}{1 - M^2}, \qquad 0 < M < 0{\cdot}6. \tag{15}$$

3.2. COMPACT APPROXIMATION

In the limit in which the compression wave thickness ($\sim R/M$) is very much larger than the tunnel diameter, it is possible to use the so-called *compact* approximation to Green's function. This was done in reference [10], where it was shown that

$$G(\mathbf{x}, \mathbf{x}'; t-\tau) \approx \frac{c_o}{2\mathscr{A}} \{H(t-\tau-|\phi^*(\mathbf{x})-\phi^*(\mathbf{x}')|/c_o) - H(t-\tau+(\phi^*(\mathbf{x})+\phi^*(\mathbf{x}'))/c_o)\}, \tag{16}$$

where $\phi^*(\mathbf{x})$ is that solution of Laplace's equation that describes a hypothetical incompressible, irrotational flow *out* of the tunnel mouth, normalized such that

$$\phi^*(\mathbf{x}) \approx x - \ell, \qquad \text{as } x \to -\infty \text{ inside the tunnel,}$$

$$\approx O(1/|\mathbf{x}|), \qquad \text{as } |\mathbf{x}| \to \infty \text{ outside the tunnel.}$$

The formulae are applicable for any tunnel whose interior cross-sectional area ultimately becomes constant and equal to $\mathscr{A}$. The length ℓ is the tunnel-mouth "end-correction" [13], which has order of magnitude $\sim\sqrt{\mathscr{A}}$, the precise value being determined by the tunnel entrance geometry. $\phi^*(\mathbf{x})$ varies continuously through the tunnel mouth, increasing from $-\infty$ at $x = -\infty$ within the tunnel, to zero at $|\mathbf{x}| = \infty$ outside. It is numerically of order $\sqrt{\mathscr{A}}$ in the neighbourhood of the mouth, where its rate of change depends on the shape of the mouth and its environment. The approximation (16) is uniformly valid when regarded as a function of either $\mathbf{x}$ or $\mathbf{x}'$ provided at least one of these points lies within the tunnel at a large distance compared to the tunnel diameter.

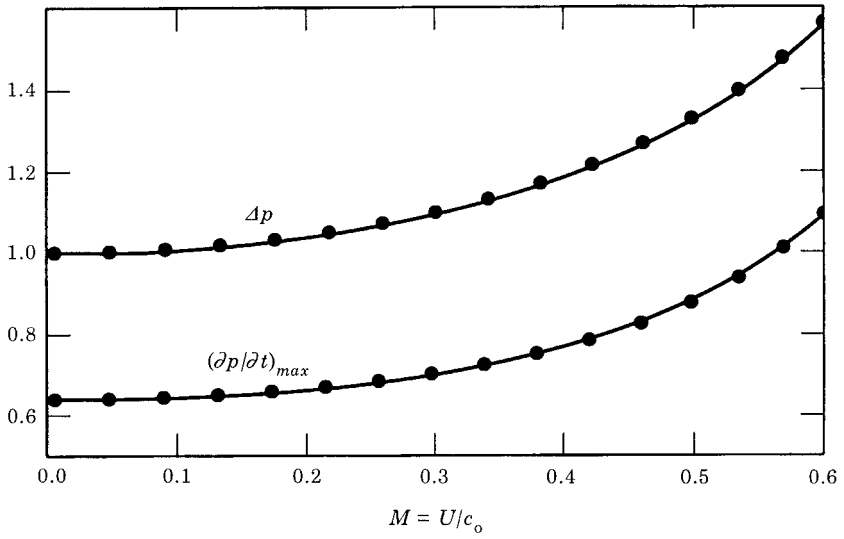

Figure 3. Predicted dependence on Mach number of the pressure rise $\Delta p/(\rho_o U^2 \mathscr{A}_o/\mathscr{A})$ and the maximum pressure gradient $(\partial p/\partial t)_{\max}/(\rho_o U^3 \mathscr{A}_o/R\mathscr{A})$ for a snub nosed train approximated by a point source. The dotted curves are the corresponding predictions of equations (14) and (15).

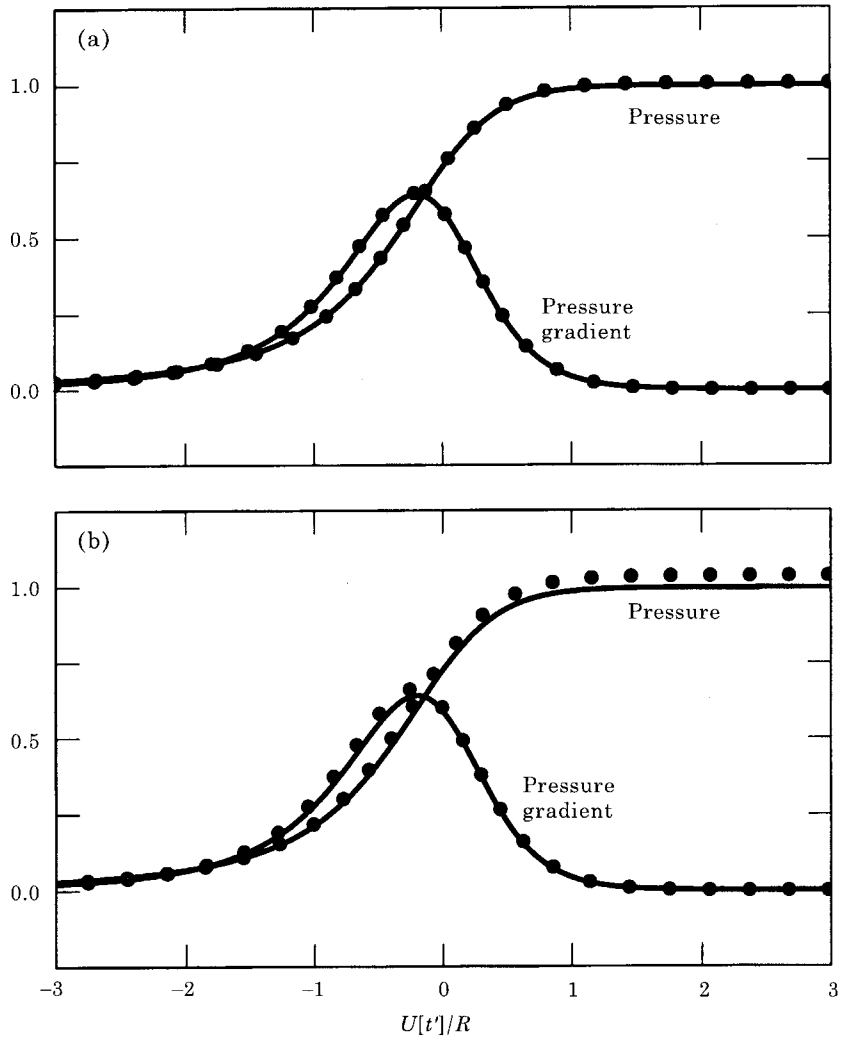

Figure 4. Comparison of the compact approximation (17) for the pressure $p/(\rho_o U^2 \mathscr{A}_o/\mathscr{A})$ and pressure gradient $(\partial p/\partial t)/(\rho_0 U^3 \mathscr{A}_o/R\mathscr{A})$ (—) for a train modelled by a point source with exact predictions based on equation (11) (●●●●) for (a) $M = 0{\cdot}1$, (b) 0·2; $t' = t - 0{\cdot}61R/c_o$.

Proceeding by the method of section 2, writing the solution of the wave equation as in equation (3), the compression wave pressure gradient is now found to be given by (see reference [10] for details)

$$\frac{\partial p}{\partial t}(x, t) \approx -\frac{\rho_o U^2}{\mathscr{A}} \int q(x' + U[t'], y', z') \frac{\partial^2 \phi^*}{\partial x'^2}(\mathbf{x}')\, \mathrm{d}^3\mathbf{x}',$$

where

$$[t'] = t + (x - \ell)/c_o. \tag{17}$$

The solid curves in Figure 4 are predictions of this formula for the snub nosed train modelled by the point source $q(\mathbf{x}) = U\mathscr{A}_o\delta(\mathbf{x})$ entering the circular cylindrical tunnel, which has the end-correction $\ell \approx 0{\cdot}61R$. The dotted curves are the results of the exact

calculation given by equation (11) for Mach numbers $M = 0{\cdot}1$ and $0{\cdot}2$. Predictions of the compact approximation are seen to be adequate for practical purposes; indeed, according to Figure 3 the error in the compact approximation does not exceed 5% until $M > 0{\cdot}3$.

4. SCALE MODEL EXPERIMENTS

Consider next the axisymmetric model "trains" investigated experimentally by Maeda *et al*. [4] using the arrangement illustrated schematically in Figure 1. The nose profiles studied included the cone, and the paraboloid and ellipsoid of revolution, with respective cross-sectional areas given by

$$\frac{\mathscr{A}_T(x)}{\mathscr{A}_o} = \frac{x^2}{L^2}, \frac{x}{L}, \frac{x}{L}\left(2 - \frac{x}{L}\right), \qquad 0 < x < L,$$

$$= 1, \qquad x \geqslant L,$$

and corresponding source densities Q (equation (1))

$$Q(x) = \frac{2x}{L^2}, \frac{1}{L}, \frac{2}{L}\left(1 - \frac{x}{L}\right), \qquad 0 < x < L,$$

$$= 0, \qquad \text{elsewhere.} \tag{18}$$

Typical predictions of the compression wave pressure and pressure gradient from equation (11) are illustrated in Figures 5 and 6, respectively, for $M = 0{\cdot}2$, $0{\cdot}4$ and $L/R = 2$ when the train travels along the axis of the cylinder ($y_T = 0$). Corresponding non-dimensional pressure gradients $(\partial p/\partial t)/(\rho_o U^3 \mathscr{A}_o/R\mathscr{A})$ increase by about 15% when M increases from $0{\cdot}2$ to $0{\cdot}4$, in agreement with the empirical formula (15). The three pressure gradient profiles always have a common point of intersection because the source strength for the paraboloid is the mean of those for the cone and the ellipsoid. Also, the compression wave pressure rise $\Delta p = \rho_o U^2(\mathscr{A}_o/\mathscr{A})/(1 - M^2)$ is the same for all three models (i.e., areas under the pressure gradient curves are equal), in accordance with the remark in section 3 following equation (14).

The data points plotted in Figure 7 are for measured values of the pressure gradient $\partial p/\partial t$ at about 1 m from the inlet of a thin walled, circular cylindrical tunnel 7 m long and radius $R = 0{\cdot}0735$ m. Model trains of aspect ratio $h/L = 0{\cdot}2$ and area ratio $\mathscr{A}_o/\mathscr{A} = 0{\cdot}116$ were projected along the tunnel axis at $U = 230$ km/h ($M = 0{\cdot}188$). For all of the pressure gradient profiles, the peak values of $\partial p/\partial t$ calculated from equation (11) are found to be just under 5% *smaller* than the corresponding measured value. For the ellipsoid, the peak measured pressure gradient is about 275 kPa/s; the calculated value is 263 kPa/s. The solid curves in Figure 7 represent the theoretical predictions increased uniformly by multiplication by the ratio $275/263 \approx 1{\cdot}045$. Also the retarded time origin of the theoretical curves has been shifted so that the peaks for theory and experiment coincide for the *ellipsoid*. This adjustment gives excellent overall agreement for all three cases.

The small systematic difference between theory and experiment is probably associated with the approximation (1), in which the displacement effect of the train is modelled by a line source distributed along the axis of symmetry of the nose. A more accurate representation would involve the placement of monopole sources on the actual surface of the nose. The closer proximity of these sources to the edges of the tunnel mouth during entry of the train into the tunnel should account for most of the 5% error.

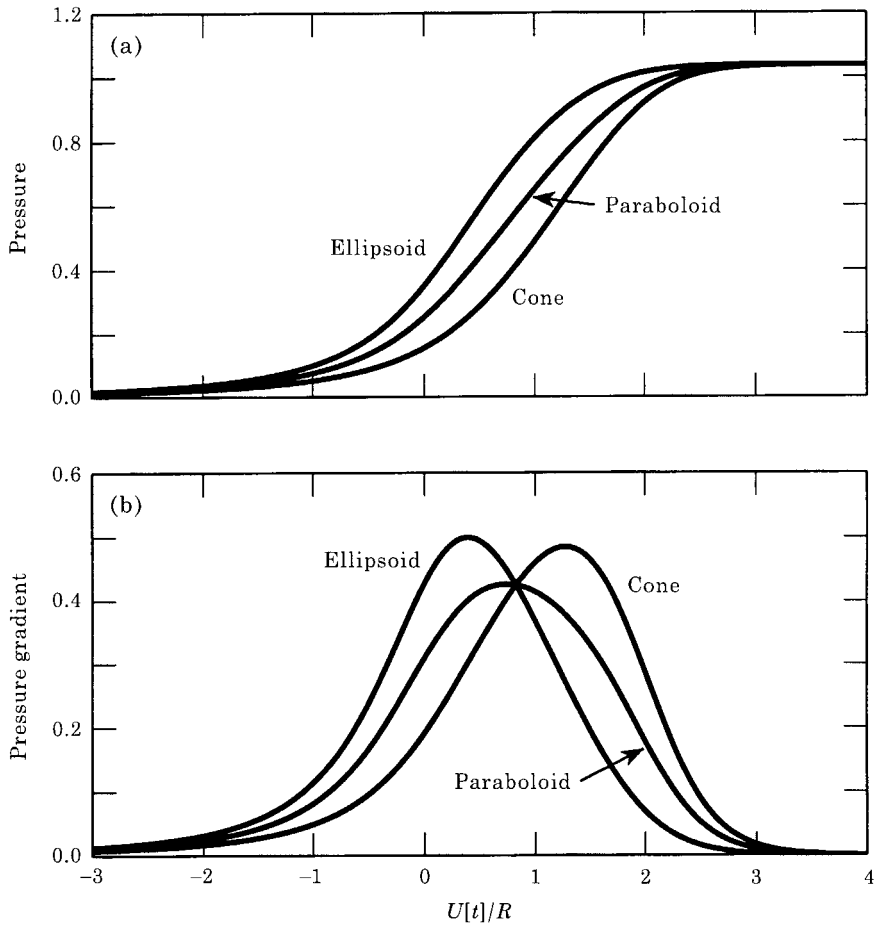

Figure 5. (a) Compression wave pressure $p/(\rho_o U^2 \mathscr{A}_o/\mathscr{A})$ and (b) pressure gradient $(\partial p/\partial t)/(\rho_0 U^3 \mathscr{A}_o/h\mathscr{A})$ for model conical, paraboloidal and ellipsoidal nose profiles when $M = 0{\cdot}2$ and $L/R = 2$.

Figure 7 exhibits the largest differences between theory and experiment in the tail region, beyond $t = 0{\cdot}01$ s. Inspection of the data given in reference [4] reveals that these tails extend out to $t \approx 0{\cdot}014$ s. Whereas the areas bounded by the theoretical curves and the time axis are equal, and so, therefore, are the net predicted pressure rises Δp, the presence of these tails is responsible for small differences in the measured values of Δp for the three cases. The overall effect is that the measured pressure rises are about 12% larger than the prediction of 0·62 kPa obtained after increasing the theoretical result by 4·5%. The tails are presumably the result of a reverberant wave generated by the compressed air projection mechanism used in the experiments, or may be attributable to boundary layers or separation, either behind the compression wave or on the train.

5. CONCLUSION

Future high-speed trains are expected to operate at Mach numbers close to 0·4. At such speeds, special consideration must be given to controlling the impact of the large amplitude compression wave generated when the train enters a tunnel. The expansion wave reflected from the far end of the tunnel, and waves reflected from tunnel discontinuities, can be a

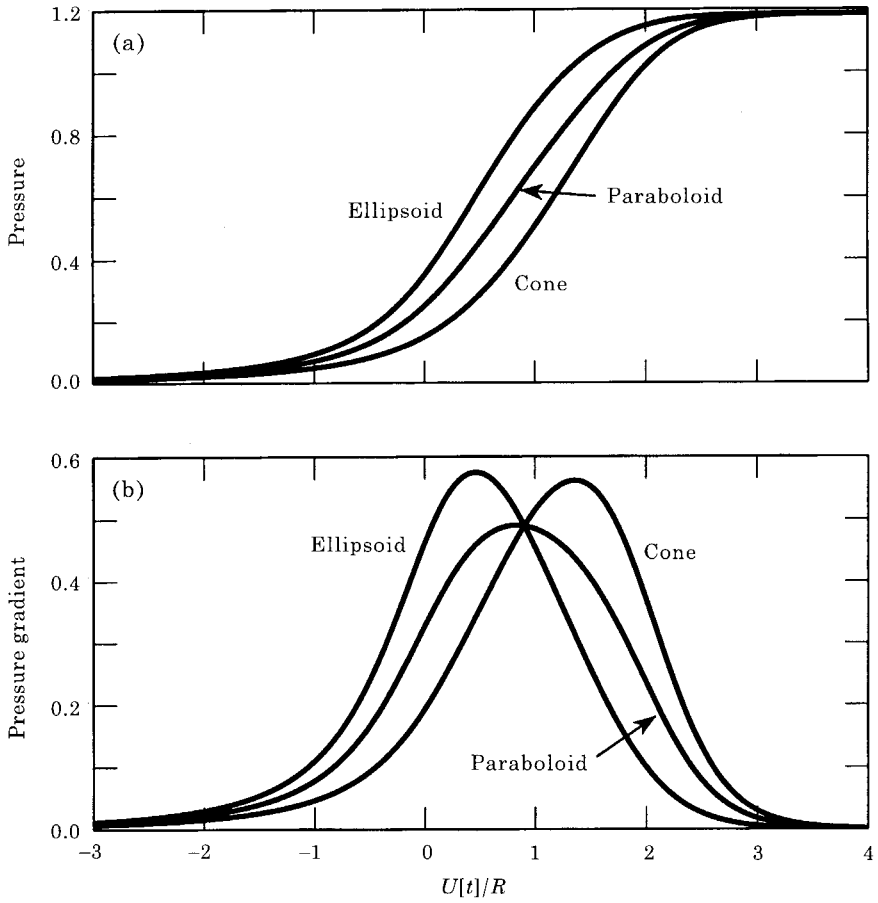

Figure 6. (a) Compression wave pressure $p/(\rho_o U^2 \mathscr{A}_o/\mathscr{A})$ and (b) pressure gradient $(\partial p/\partial t)/(\rho_0 U^3 \mathscr{A}_o/h\mathscr{A})$ for model conical, paraboloidal and ellipsoidal nose profiles when $M = 0{\cdot}4$ and $L/R = 2$.

serious source of passenger discomfort. Similarly, non-linear steepening of the compression wave in a very long tunnel can exacerbate environmental problems associated with the impulsive *micro-pressure wave* radiated from the end of the tunnel.

Full scale numerical simulations of tunnel–train interactions will be necessary to predict high Mach number compression wave characteristics in practical situations. However, analytical predictions for simple geometries can be used to guide and interpret results of scale model tests. In this paper, such predictions are made of the influence of train Mach number M on the compression wave generated when an axisymmetric model train is projected into a thin-walled circular cylindrical tunnel. For a train whose cross-sectional area is small, ($\mathscr{A}_o/\mathscr{A} < 0{\cdot}2$, for example) Mach number effects become significant when M exceeds about 0·25. Empirical formulae valid up to $M = 0{\cdot}6$ have been given for predicting the pressure rise across the wavefront and the initial maximum pressure gradient (which determines the amplitude of the micro-pressure wave). These results are derived by representing the nose of the train by a distribution of monopole sources along its axis of symmetry, and by use of the exact acoustic Green's function for a semi-infinite, circular cylindrical tunnel. The theory has been validated for this case by comparison with model scale experiments conducted by Maeda *et al*. [4]; pressure gradient predictions are found to be within 5% of the observations.

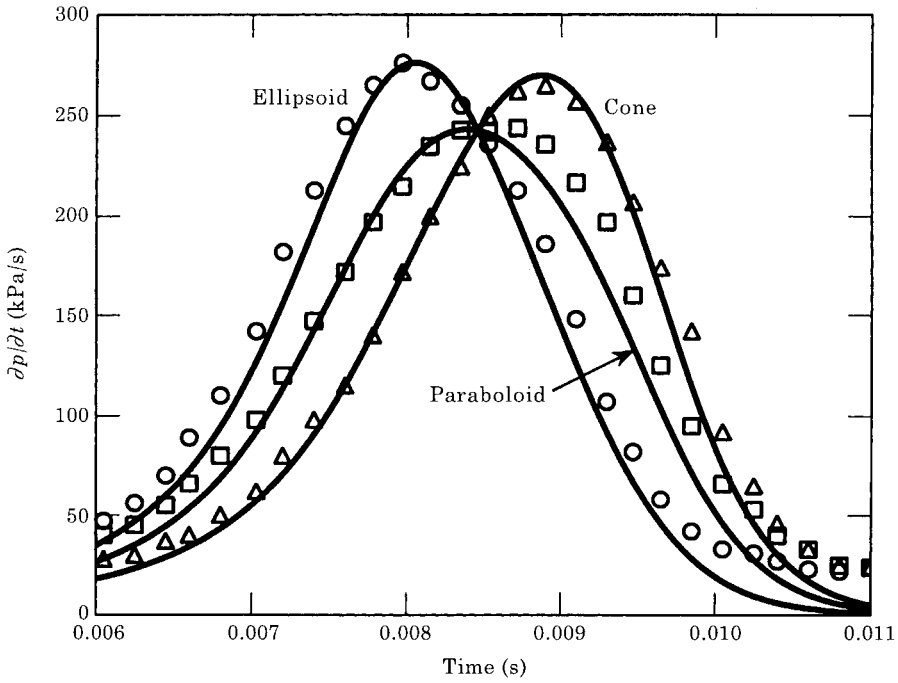

Figure 7. Comparison of measured [4] and predicted (—) pressure gradients $\partial p/\partial t$ for model conical (△), paraboloidal (□) and ellipsoidal (○) nose profiles when $\mathscr{A}_o/\mathscr{A} = 0{\cdot}116$, $R = 0{\cdot}0735$ m, $M = 0{\cdot}188$ and $h/L = 0{\cdot}2$. The theoretical predictions have been increased by 4·5 %.

REFERENCES

1. S. Ozawa, Y. Morito, T. Maeda and M. Kinosita 1976 *Railway Technical Research Institute Report* 1023 (in Japanese). Investigation of the pressure wave radiated from a tunnel exit.
2. S. Ozawa 1979 *Railway Technical Research Institute Report* 1121 (in Japanese). Studies of the micro-pressure wave radiated from a tunnel exit.
3. S. Ozawa, T. Maeda, T. Matsumura, K. Uchida, H. Kajiyama and K. Tanemoto 1991 in *Aerodynamics and Ventilation of Vehicle Tunnels*, 253–266. Oxford: Elsevier Science. Countermeasures to reduce micro-pressure waves radiating from exits of Shinkansen tunnels.
4. T. Maeda, T. Matsumura, M. Iida, K. Nakatani and K. Uchida 1993 in *Proceedings of the International Conference on Speedup Technology for Railway and Maglev Vehicles*, *Yokohama*, *Japan*, 315–319. Effect of shape of train nose on compression wave generated by train entering tunnel.
5. M. Iida, T. Matsumura, K. Nakatani, T. Fukuda and T. Maeda 1996 *Institute of Mechanical Engineers Paper* C514/015/96. Optimum nose shape for reducing tunnel sonic boom.
6. T. Ogawa and K. Fujii 1994 in *Proceedings of the Shock Wave Symposium*, *Chiba*, *Japan* (sponsored by the Japan Society of Shock Wave Research, the Institute of Fluid Science at Tohoku University, and The Institute of Space and Astronautical Science). Effect of train shape on a compression wave generated by a train moving into a tunnel.
7. T. Ogawa and K. Fujii 1994 *Computational Fluid Dynamics Journal* **3**, 63–82. Numerical simulation of compressible flows induced by a train moving into a tunnel.
8. T. Ogawa and K. Fujii 1996 in *Proceedings of the European Community Conference on Computational Methods in Applied Sciences*. New York: Wiley. Prediction and alleviation of a booming noise created by a high-speed train moving into a tunnel.
9. T. Ogawa and K. Fujii 1997 *Journal of Computers and Fluids* **26,** 565–585. Numerical investigation of three dimensional compressible flows induced by a train moving into a tunnel.
10. M. S. Howe 1997 *Proceedings of the Royal Society A* (in press). The compression wave produced by a high-speed train entering a tunnel.

11. M. Liang, T. Kitamura, K. Matsubayashi, T. Kosaka, T. Maeda, N. Kudo and S. Yamada 1994 *Journal of Low Frequency Noise and Vibration* **13**, 39–47. Active attenuation of low frequency noise radiated from tunnel exit of high speed train.
12. J. Sawada 1993 in *Proceedings of the International Conference on Speedup Technology for Railway and Maglev Vehicles*, *Yokohama*, *Japan*, 1–3 (organized by The Japan Society of Mechanical Engineers). Role of high speed railways in Japan.
13. Lord Rayleigh 1945 *The Theory of Sound*, Volume 2. New York: Dover.
14. A. D. Pierce 1989 *Acoustics*, *An Introduction to its Principles and Applications*. American Institute of Physics.
15. B. Noble 1958 *Methods Based on the Wiener-Hopf Technique for the Solution of Partial Differential Equations*. Oxford: Pergamon Press. (Reprinted in 1988 by Chelsea Publishing Company, New York.)
16. M. Abramowitz and I. A. Stegun (editors) 1970 *Handbook of Mathematical Functions* (ninth corrected printing). U.S. Department of Commerce, National Bureau of Standards Applied Mathematics Series No. 55.